Effects of Surface Nonuniformities on the Mean Transverse Energy from Photocathodes

Siddharth Karkare* and Ivan Bazarov

CLASSE, Cornell University, Ithaca, New York 14853, USA

(Received 24 March 2015; revised manuscript received 29 July 2015; published 24 August 2015)

The performance of photoinjectors is limited by the lowest value of the mean transverse energy of the electrons obtained from photocathodes. The factors that influence the mean transverse energy are poorly understood. In this paper, we develop models to calculate the effect of spatial work-function variations and subnanometer-scale roughness and surface defects on the mean transverse energy. We show that these can limit the lowest value of mean transverse energy achieved and that atomically perfect surfaces will be required to further reduce the mean transverse energy obtained from photocathodes.

DOI: 10.1103/PhysRevApplied.4.024015

I. INTRODUCTION

Photoinjectors provide electron beams for most fourth-generation light sources like energy-recovery linacs and free-electron lasers and ultrafast electron diffraction (UED) setups. For light-source applications, the mean transverse energy (MTE) of electrons emitted from the photocathode limits the beam brightness obtained from photoinjectors [1]. For UED applications, the transverse coherence length of the electron beam also tends to be limited by the MTE obtained from photocathodes [2,3]. The transverse coherence length sets the maximum size of the crystal unit cell for which a diffraction pattern can be resolved. Thus, reducing the MTE from photocathodes can result in brighter electron beams and can allow UED of crystals with larger unit cells, for example, proteins.

Intrinsic (sometimes also called "thermal") emittance, which is the volume occupied by the electron beam in phase space, is a more familiar quantity to accelerator physicists. The normalized thermal emittance can be related to the MTE and the rms laser spot size on the cathode ($\sigma_{l,x}$) through the relation $\epsilon_{n,x} = \sigma_{l,x}\sqrt{\mathrm{MTE}/m_e c^2}$, where m_e is the mass of an electron and c is the speed of light.

The theoretical lower limit to the MTE, given by a disorder-induced scattering after emission, is 1–2 meV [4]. The smallest MTE demonstrated is in the 25–40 meV range from GaAs activated to negative electron affinity (NEA) using Cs and NF_3 [5] under infrared illumination or from antimony films using near-photoemission-threshold wavelengths [6]. However, NEA GaAs under infrared illumination has a very large response time in the 100 ps range [5], and antimony or other metals have very small quantum efficiency near the photoemission threshold, sometimes making them impractical for use in a photoinjector. In most photoinjectors, MTE in the range of 100 meV to 1 eV is obtained from photocathodes [7]. Before reaching the theoretical limit, nearly 2 orders of magnitude improvement in MTE may be possible by engineering photocathode materials [8–10] that have smaller MTE with high quantum efficiencies and quick response times. However, no theory exists that can explain the observed MTE from photocathodes satisfactorily; several major discrepancies still exist.

One theory states that the MTE obtained from metal photocathodes is nearly one-third the excess energy [11]. Here, the excess energy is defined as the energy difference between the incident photon and the work function of the material. An extension of this theory states that the MTE approaches the lattice temperature energy (25 meV at room temperature–thus the name "thermal" sometimes used with emittance) as the excess energy tends to zero (near the photoemission threshold) [12]. This theory produces reasonable agreement with experimental data for metal and thin-film alkali antimonide photocathodes [6,13–15]. However, this theory does not take into account the effects of band structure, conservation of transverse momentum during emission, and the effective mass of electrons in the lattice. Another theory does include the does include the effective mass of electrons in the lattice and the conservation of transverse momentum to predict the photoemission from metals [16,17]. In NEA GaAs cathodes, the conservation of transverse momentum and the small effective mass of electrons in the Γ valley should result in a MTE below 20 meV in infrared-green wavelengths [18,19]. However, experimental results show a MTE of 25–120 meV in this wavelength range [5]. This discrepancy has been attributed to a surface scattering mechanism that redistributes the emitted electrons uniformly in the polar angle [18] or causes the Γ-valley electrons near the surface to have an effective mass equal to the mass of a free electron [20]. However, no physical reason for this scattering mechanism has been identified.

To add to the complexity, the surfaces of frequently used photocathode materials are far from perfect. Photocathode surfaces often display roughness on the scales of tens of nanometers [21–23]. Single-crystal photocathodes which

*ssk226@cornell.edu

are atomically flat may exhibit surface reconstructions, atomic-scale surface defects, and monolayer adsorbates [24]. The effect of greater than 10-nm-scale roughness on MTE has been studied [22,23,25,26]. However, the effect of subnanometer-scale surface defects, surface reconstructions, and adsorbates on MTE remains unexplored.

Work-function variations ranging from 1 meV to hundreds of meV over less than nanometer scale to micron scale (along the cathode surface) can be caused due to atomic defects, atomic steps, surface reconstructions, localized charging, localized strains, grain boundaries, and adsorbates [27–30]. The effect of such work-function variations on MTE also remains unexplored.

In this paper, we investigate the effect of these work-function variations and surface nonuniformities to show that it is important to consider their effects to achieve lower MTE. First, we treat the effect of spatial work-function variations on emitted electrons in a classical manner. The classical treatment is valid whenever the de Broglie wavelength of emitted electrons is much smaller than the scale of the spatial work-function variation. Electric fields are formed in the vacuum region close to the cathode surface because of the work-function variations. These electric fields deflect the emitted electrons and cause the MTE to increase. We estimate the rise in MTE due to these electric fields for a sinusoidal variation in the work function. We show that the effect of work-function variation can be significant but reduces with an increase in the kinetic energy of the emitted electron.

Next, we formulate a quantum-mechanical emission model to include the effects of surface nonuniformities in the case when the de Broglie wavelength of the emitted electrons is similar to the scale of the surface nonuniformities. Such nonuniformities include atomic steps and defects, surface reconstructions, work-function variations on a nanometer scale, and adsorbates.

Finally, using the quantum-mechanical formulation and the example of photoemission from activated GaAs photocathodes, we show that subnanometer-scale roughness which can be comprised of atomic steps, surface defects, and surface reconstructions can limit the minimum MTE attainable. We also show that these can account for the surface scattering mechanisms responsible for increasing the theoretically predicted MTE from NEA GaAs photocathodes.

II. CLASSICAL TREATMENT

Generally, electrons emitted from photocathodes have kinetic energies in the 10 meV to 1 eV range [7]. This results in a de Broglie wavelength of 1–10 nm. Thus, spatial variations in work functions at a scale much greater than 10 nm can be treated in a classical manner. Work-function variations at these large spatial scales can be caused due to localized surface charging, localized strains, patches of surface adsorbates, and different grain orientations [27–30]. There have been previous attempts to study the effects of such patchy work-function surfaces on low-energy electron reflection [31], thermionic emission [32], and field emission [33].

The spatial variations in a work function cause transverse (parallel to the cathode surface) electric fields. These give a transverse kick to the emitted electrons and increase the MTE of the cathode. In this section, we calculate the electric fields formed due to a sinusoidal work-function variation and estimate the effect they have on the MTE.

A similar effect, in which the transverse electric fields are caused due to the surface roughness of the cathode, has been studied [25,26,34]. The calculation given below to estimate the effects of work-function variation on MTE closely follows the surface roughness effect calculation.

A. Details of model and calculation

The potential of an electron right outside an electrode is the negative of bias applied to the electrode in volts plus the work function in eV. Thus, variation in the work function essentially causes a variation in the surface potential of the electrode. In any photoinjector, a cathode is placed in a very high (approximately 1–50 MV/m) longitudinal electric field. The variations in the surface potential cause the longitudinal electric field very close to the cathode surface to deform and acquire transverse components which decay rapidly as one goes away from the cathode. To model such a field, we consider a parallel-plate capacitor as shown in Fig. 1. It consists of a cathode that is grounded at $z = 0$ and a parallel anode biased to a voltage ϕ_0 at $z = L_0$. Thus, the longitudinal electric field at

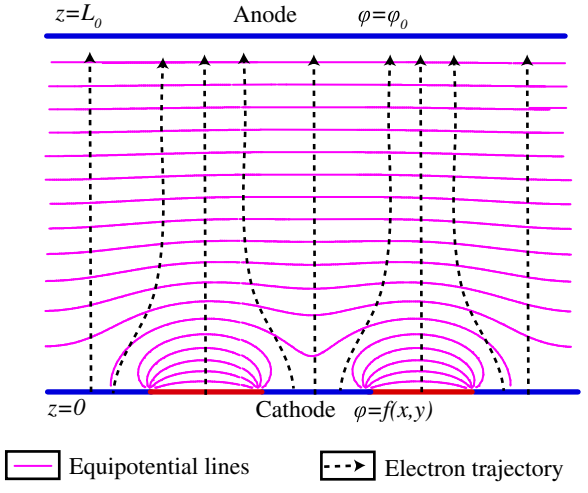

FIG. 1. Parallel-plate capacitor model to calculate the effect of variation of the work function on MTE. The equipotential lines get distorted near the cathode due to the nonuniform work function. This causes the electrons emitted from the cathode to gain transverse energy.

the cathode without the work-function variation is $E_0 = \phi_0/L_0$. Let the work-function variation on the cathode be given by $f(x,y) \ll \phi_0$. For simplicity, we approximate the work-function variation by a sinusoidal function $f(x,y) = h\sin[(2\pi/a)x]\sin[(2\pi/a)y]$, where h is the amplitude of the work-function variation and a is its spatial period.

Using the Laplace equation $\nabla^2\phi = 0$ with boundary conditions $\phi|_{z=0} = f(x,y)$ and $\phi|_{z=L_0} = \phi_0$, we can obtain ϕ in the region between the cathode and the anode as

$$\phi(x,y,z) = \phi_0\frac{z}{L_0} + h\frac{(e^{-z\gamma} - e^{(z-2L_0)\gamma})}{1-e^{-2L_0\gamma}} \times \sin\left(\frac{2\pi}{a}x\right)\sin\left(\frac{2\pi}{a}y\right), \quad (1)$$

where $\gamma = (2\sqrt{2}\pi/a)$. We also assume that $a \ll L_0$ so that the transverse electric fields (E_x and E_y) are nearly zero well before $z = L_0$. Using this approximation, the potential can be given as

$$\phi(x,y,z) = \phi_0\frac{z}{L_0} + he^{-z\gamma}\sin\left(\frac{2\pi}{a}x\right)\sin\left(\frac{2\pi}{a}y\right). \quad (2)$$

From this, the electric fields in the x, y, and z can be calculated as, respectively,

$$\begin{aligned} E_x &= \frac{2\pi}{a}he^{-z\gamma}\cos\left(\frac{2\pi}{a}x\right)\sin\left(\frac{2\pi}{a}y\right), \\ E_y &= \frac{2\pi}{a}he^{-z\gamma}\sin\left(\frac{2\pi}{a}x\right)\cos\left(\frac{2\pi}{a}y\right), \\ E_z &= -E_0 + h\gamma e^{-z\gamma}\sin\left(\frac{2\pi}{a}x\right)\sin\left(\frac{2\pi}{a}y\right). \end{aligned} \quad (3)$$

The transverse velocities (v_x and v_y) can be calculated by integrating the equations of motion. We integrate the equations of motion numerically using an eight-stage symplectic implicit integrator [35]. Electrons are launched from a fine grid of spacing $a/40$ on the surface to obtain a fine sampling of all areas of the surface. The electrons are launched perpendicular to the surface with kinetic energy K. The initial transverse velocity and energy are set be zero. The electrons are tracked in the electric field given by Eq. (3), and the trajectories are calculated till the point where the transverse electric fields become negligible and the transverse velocities are constant. The mean transverse energy is then calculated by averaging over the transverse energy of all the electrons. As the initial transverse velocities and energies are zero, this analysis gives us only the contribution of work-function nonuniformities to the MTE.

An analytic expression for the MTE can also be obtained by making the assumption $h/a \ll E_0$ and that the change in x and y is negligible compared to a. With these assumptions, the expressions for the electric fields become

$$\begin{aligned} E_x &= \frac{2\pi}{a}he^{-z\gamma}\cos\left(\frac{2\pi}{a}x_0\right)\sin\left(\frac{2\pi}{a}y_0\right), \\ E_y &= \frac{2\pi}{a}he^{-z\gamma}\sin\left(\frac{2\pi}{a}x_0\right)\cos\left(\frac{2\pi}{a}y_0\right), \\ E_z &= -E_0, \end{aligned} \quad (4)$$

where x_0 and y_0 are the coordinates of the point from where the electron is launched.

Under these approximations, the equations of motion can be integrated analytically to obtain the final transverse velocities v_x and v_y. The MTE can by calculated by averaging the transverse kinetic energy over the entire surface as $\text{MTE} = \frac{1}{2}m_e[\iint(v_x^2+v_y^2)dxdy/\iint dxdy]$. The MTE thus obtained can be given by the analytic expression

$$\text{MTE} = \frac{\pi^2h^2e}{4\sqrt{2}aE_0}e^{-(\beta^2/2\alpha)}\text{erfc}^2\left(\frac{\beta}{2\sqrt{\alpha}}\right), \quad (5)$$

where $\alpha = (\sqrt{2}\pi eE_0/am_e)$ and $\beta = (4\pi\sqrt{K}/a\sqrt{m_e})$.

B. Results

Figure 2 shows the MTE calculated by numerically tracking electron trajectories for initial kinetic energies (K) of 20 and 60 meV and $a = 100$ nm. Figure 2(a) shows the MTE calculated at zero electric field as a function of h for $K = 20$ meV. We can see that values of h as low as 0.1 V can result in MTE higher than 20 meV.

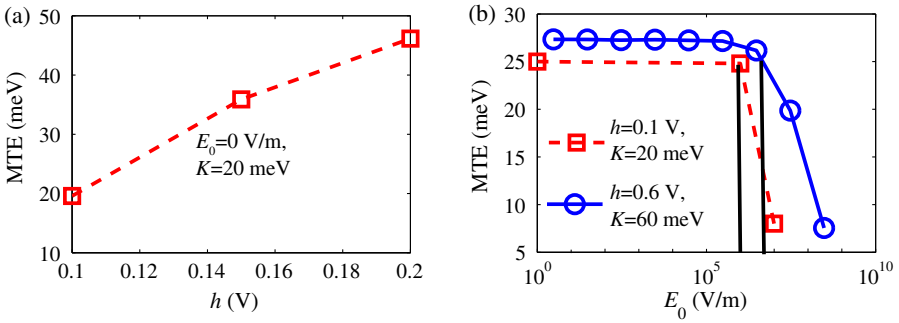

FIG. 2. (a) Variation of MTE with h. The external electric field is set to zero for these calculations. (b) Variation of the MTE with the electric field E_0. The value of a is set to 100 nm for these calculations. h/a for the red curve is 1 MV/m and for the blue curve is 6 MV/m (shown by the black lines). The MTE is nearly independent of the electric field when $E_0 < h/a$; beyond that, it reduces sharply with the electric field.

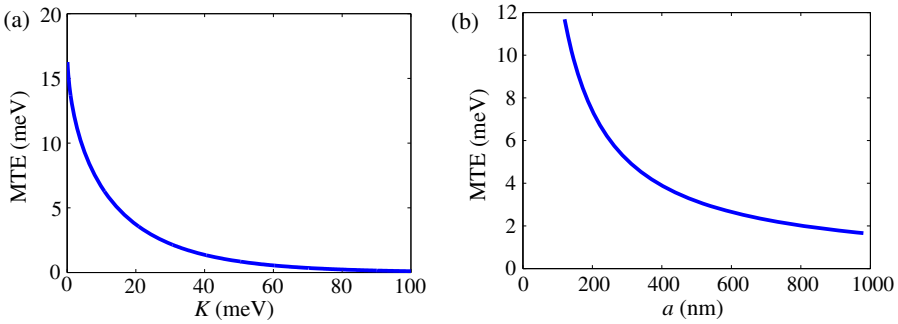

FIG. 3. (a) Variation of MTE with the initial kinetic energy. $E_0 = 10$ MV/m, $h = 0.1$ V, and $a = 100$ nm. (b) Variation of MTE with the period a. $E_0 = 10$ MV/m, $h = 0.1$ V, and $K = 1$ meV.

Figure 2(b) shows the variation of MTE with an electric field for two cases: $h = 0.1$ V and $K = 20$ meV; $h = 0.6$ V and $K = 60$ meV. We can see that for both cases the MTE is nearly constant with the electric field (E_0) so long as the electric field is below h/a (shown by the black lines in the figure). If $E_0 < h/a$, the first term in the expression for E_z in Eq. (3) can be ignored, making the electric field near the cathode surface independent of E_0. Hence, the MTE does not vary much with E_0 in this regime. However, as the electric field rises beyond h/a, the electrons are extracted away from the cathode surface more quickly. This gives them less time to interact with the transverse electric fields close to the surface, and hence the MTE reduces. This reduction in MTE with the electric field should be easily observable with electric fields in the range of 1–10 MV/m if the MTE is indeed limited by work-function nonuniformities on a classical scale. Such a change with the electric field is contrary to the change expected due to the 10–100-nm-scale surface roughness [25,26]. Because of the surface roughness effect, the MTE increases with increasing the electric field.

MTE also reduces with an increase in the initial kinetic energy (K) and an increase in the period a. Figures 3(a) and 3(b) show the variation of MTE with the initial kinetic energy and the period a, respectively, for $h = 0.1$ V and $E_0 = 10$ MV/m. These parameters are such that the approximations made to estimate the MTE in Eq. (5) are valid. The MTE in Fig. 3 is calculated from this equation.

In short, we see that work-function variations of approximately 0.1 eV over a scale of approximately 100 nm can limit the MTE to 20–30 meV if the kinetic energy of the emitted electrons is near 20 meV. This is often the case with near-threshold photoemission, where the excess energy and hence the kinetic energy of emitted electrons is approximately 25 meV (thermal energy at room temperature). Work-function variations of similar magnitudes have been experimentally observed on various surfaces due to localized surface charging, localized strains, patches of surface adsorbates, and different grain orientations [27–30]. Hence, in order to obtain MTE of less than 20 meV, it will be necessary to ensure the spatial uniformity of cathode work functions. It is also important to measure the work-function variations on practical cathode surfaces to the resolution of a micron to a nanometer.

III. QUANTUM TREATMENT

In this section, we develop an emission model that takes into account surface nonuniformities of spatial scales less than or comparable to the de Broglie wavelength of the emitted electrons and show how conservation of transverse momentum can be violated in their presence.

A. Emission model

The emission model described here assumes a semiconductor cathode; however, it can easily be extended to metallic cathodes.

The model assumes Spicer's three-step process of photoemission [36]. The first two steps of electron excitation from the valence band to the conduction band and subsequent electron transport to the surface in the conduction band are well understood [18]. Here, we discuss the last step of emission to include the effects of surface nonuniformities.

Figure 4(a) shows the potential used to describe the cathode-vacuum interface. The electrons approach the surface in the form of plane waves with crystal momentum $\mathbf{k}_{\text{in}}$ and energy E_c. We assume that the energy and the crystal momentum are related via the parabolic, spherical dispersion relation

$$E_c = \frac{\hbar^2 |\mathbf{k}_{\text{in}}|^2}{2m^*}, \tag{6}$$

where m^* is the effective mass of the electron inside the cathode. The potential within the cathode and in vacuum is assumed to be constant. The interface is represented by a potential $g(x, y, z)$ along with a step of height V. The potential $g(x, y, z)$ includes all interface effects, transverse variations of the potential due to surface nonuniformities, and defects and electric fields due to work-function variations. $g(x, y, z)$ is zero in the cathode bulk and in vacuum but is nonzero in the interface region. The incoming electron wave gets scattered due to the potential $g(x, y, z)$. Part of the incoming wave gets reflected, and the rest gets transmitted into vacuum. In this study, we assume a field-free region in the vacuum. This approximation is true for small electric fields generally found in dc guns.

We approximate the wave function of the incoming electron with a plane wave $\psi_{\text{in}} = e^{i(\mathbf{k}_{\text{inr}} \cdot \mathbf{r} + k_{1\text{in}z} z)}$, where

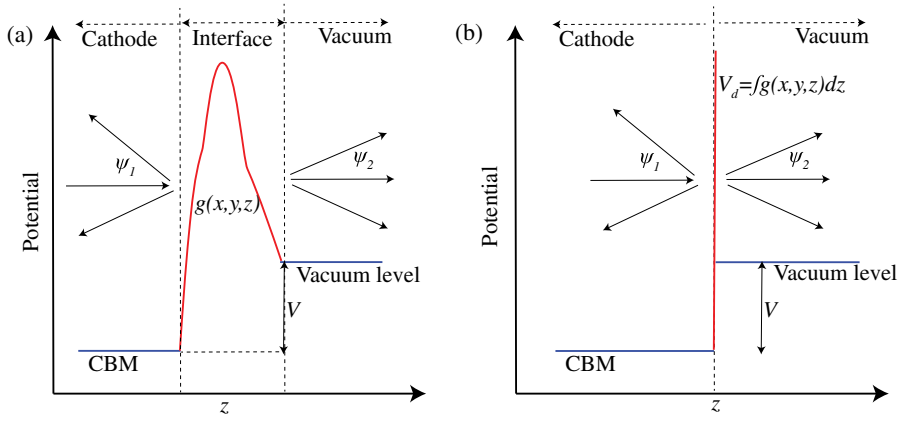

FIG. 4. (a) Potential to model the surface nonuniformities along with the incoming and scattered wave functions. (b) δ-function approximation to the potential used to account for surface nonuniformities.

$\mathbf{k}_{\mathrm{in}\mathbf{r}} = k_{\mathrm{in}x}\vec{\mathbf{x}} + k_{\mathrm{in}y}\vec{\mathbf{y}}$ is the transverse component and $k_{1\mathrm{in}z}\vec{\mathbf{z}}$ is the longitudinal component of the wave vector $\mathbf{k}_{\mathrm{in}}$ and $\mathbf{r}$ is the position vector in the transverse direction.

The challenge is to calculate the scattering of the incoming plane wave due to the interface potential $g(x,y,z)$. A similar problem has been studied extensively to model electron transport across semiconductor heterojunctions [37–42]. The most general solution to this problem is obtained by solving the Lippmann-Schwinger equation [37,43]. Solutions using a tight-binding-like approach [38–40] and a transfer-matrix approach have also been attempted [41].

Here, we simplify this problem by replacing the interface potential $g(x,y,z)$ by a δ-function whose height varies in x and y and is given by $V_d(x,y)=\int g(x,y,z)dz$. Such a simplification is valid when the interface region is much smaller than the wavelength of the emitted electrons. Figure 4(b) shows the potential with this δ-function approximation. The Hamiltonian for this system can be written as

$$H = -\frac{\hbar^2}{2}\nabla\left(\frac{1}{m}\nabla\right) + VS(z) + V_d(x,y)\delta(z), \quad (7)$$

where $m = m^*$ if $z < 0$ and $m = m_e$ if $z \geq 0$ and $S(z)$ is the Heaviside function.

$V_d(x,y)$ can be expanded in terms of its Fourier components as

$$V_d(x,y) = \sum_{\eta} V_{\mathbf{k}_{r\eta}} e^{i(\mathbf{k}_{r\eta}\cdot\mathbf{r})}. \quad (8)$$

The wave function of the incoming and the reflected electrons within the photocathode can then be written as

$$\psi_1 = \psi_{\mathrm{in}} + \alpha_{\mathbf{k}_{\mathrm{in}r}} e^{i(\mathbf{k}_{\mathrm{in}r}\cdot\mathbf{r} - k_{1\mathrm{in}z\eta}z)} + \sum_{\eta} e^{i(\mathbf{k}_{r\eta}\cdot\mathbf{r} - k_{1z\eta}z)}, \quad (9)$$

where $\mathbf{k}_{r\eta}$ and $k_{1z\eta}\vec{\mathbf{z}}$ are the transverse and longitudinal components, respectively, of the wave vectors into which the incoming electron wave is scattered due to reflection from the barrier V_d and $\alpha_{\mathbf{k}_{r\eta}}$ are the probability coefficients for the respective scattered wave vectors.

The wave function of the electrons transmitted into vacuum can be written as

$$\psi_2 = (1+\alpha_{\mathbf{k}_{\mathrm{in}r}})e^{i(\mathbf{k}_{\mathrm{in}r}\cdot\mathbf{r}+k_{2\mathrm{in}z}z)} + \sum_{\eta}\alpha_{\mathbf{k}_{r\eta}} e^{i(\mathbf{k}_{r\eta}\cdot\mathbf{r}+k_{2z\eta}z)}, \quad (10)$$

where $\mathbf{k}_{r\eta}$ and $k_{2z\eta}\vec{\mathbf{z}}$ are the transverse and longitudinal components, respectively, of the wave vectors into which the incoming electron wave is scattered in vacuum.

ψ_1 and ψ_2 are general and satisfy the condition $\psi_1 = \psi_2$ at $z = 0$. We assume that this scattering is elastic in nature. Hence, from the conservation of energy, all the reflected wave vectors satisfy the relation

$$\frac{\hbar^2(k_{r\eta}^2 + k_{1z\eta}^2)}{2m^*} = E_c, \quad (11)$$

and all the transmitted wave vectors satisfy the relation

$$\frac{\hbar^2(k_{r\eta}^2 + k_{2z\eta}^2)}{2m_e} = E_v = E_c - V, \quad (12)$$

$$\frac{\hbar^2(k_{\mathrm{in}r}^2 + k_{2\mathrm{in}z}^2)}{2m_e} = E_v = E_c - V, \quad (13)$$

where E_v is the kinetic energy of the electron emitted into vacuum.

Now the coefficients $\alpha_{\mathbf{k}_{\mathrm{in}r}}$ and $\alpha_{\mathbf{k}_{r\eta}}$ can be calculated by integrating the Schrödinger equation for the Hamiltonian given in Eq. (7) across the δ barrier in the z direction from 0^- to 0^+ and comparing the coefficients of the same exponents as done by Liu and Coon [42].

For a 1D sinusoidal δ barrier at the surface, given by $V_d = 2V_0\cos(k_s x)$, the set of equations to calculate α coefficients can be written in the form of a tridiagonal matrix system as

$$A\begin{pmatrix}\vdots\\ \alpha_{k_{\mathrm{in}x}-k_s}\\ \alpha_{k_{\mathrm{in}x}}\\ \alpha_{k_{\mathrm{in}x}+k_s}\\ \vdots\end{pmatrix}=\begin{pmatrix}\vdots\\ 0\\ V_0\\ R(k_{\mathrm{in}x})\\ V_0\\ 0\\ \vdots\end{pmatrix},\qquad A=\begin{pmatrix}\ddots & \vdots & \vdots & \vdots & \cdots\\ \cdots & D(k_{\mathrm{in}x}-k_s) & -V_0 & 0 & \cdots\\ \cdots & -V_0 & D(k_{\mathrm{in}x}) & -V_0 & \cdots\\ \cdots & 0 & -V_0 & D(k_{\mathrm{in}x}+k_s) & \cdots\\ \cdots & \vdots & \vdots & \vdots & \ddots\end{pmatrix},\tag{14}$$

where $R(k_x)=(i\hbar^2/2)[(k_{2z}/m_e)-(k_{1z}/m^*)]$ and $D(k_x)=(\hbar^2/2i)[(k_{2z}/m_e)+(k_{1z}/m^*)]$. k_{1z} and k_{2z} can be calculated in terms of k_r from Eqs. (11) and (12).

By solving this system, one can obtain the coefficients α in terms of the transverse wave vector of the incoming plane wave $k_{\mathrm{in}x}$ and the δ barrier at the interface. The probability of transmission into one of the scattered components with transverse wave vector $k_x \neq k_{\mathrm{in}x}$ is given by [41]

$$T_{k_x}=\frac{m^*|\alpha_{k_x}|^2(k_{2z}+k'_{2z})}{2m_e k_{1z}},\tag{15}$$

and the probability of unscattered transmission is given by

$$T_{k_{\mathrm{in}x}}=\frac{m^*|1+\alpha_{k_{\mathrm{in}x}}|^2(k_{2\mathrm{in}z}+k'_{2\mathrm{in}z})}{2m_e k_{1\mathrm{in}z}}.\tag{16}$$

The MTE due to the emission of the plane wave can then be given by

$$\mathrm{MTE}=\frac{\sum_m \frac{\hbar^2(k_{\mathrm{in}x}+mk_s)^2 T_{k_{\mathrm{in}x}+mk_s}}{2m_e}}{\sum_m T_{k_{\mathrm{in}x}+mk_s}}.\tag{17}$$

B. Example of NEA GaAs

NEA GaAs cathodes should exhibit MTE of less than 10 meV in infrared light due to the small effective mass of Γ-valley electrons and the conservation of transverse momentum during emission [18]. However, the smallest MTE measured from these cathodes is in the 25–40 meV range [5,8,44].

Using the emission model discussed in Sec. III A, we show that surface nonuniformities including atomic surface defects and surface reconstructions could explain the large MTE observed from GaAs.

In our model of the activated GaAs surface, we assume that the work function is uniform and the barrier due at the interface is negligible. The surface is modeled only by a step rise in the potential along with a sudden change in the effective mass as shown in Fig. 5(a). For the activated GaAs (100) surface, the conduction-band minimum (CBM) at the surface is approximately 0.5 V below the vacuum level [18], making the height of the step barrier $V = 0.5$ V. In our model, we assume that the band bending is very gradual and, hence, ignore any slope to the CBM near the surface. This assumption is true for very lightly doped GaAs cathodes or for layered GaAs cathodes with undoped top layer [8].

The atomic defects, steps, and reconstructions of the surface are modeled by introducing a sinusoidal surface "roughness" in the x direction. The z position of the potential step at the interface changes due to this roughness and is given by $z = t\cos[(2\pi/\lambda)x]$, where $t = 1$ nm, making the rms roughness only 0.7 nm. λ is the periodicity of the surface roughness. As shown in Fig. 5(b), this roughness can be approximated by a δ-function barrier whose height is given by $Vt\cos[(2\pi/\lambda)x] = 0.5\cos[(2\pi/\lambda)x]$ nm V. For this approximation to be valid, the wavelength of the electrons must be much larger than 1 nm. The MTE can be estimated from Eq. (17).

Figure 6(a) shows MTE as a function of the period of the surface roughness (λ) for various kinetic energies of emitted electrons. The transverse momentum of the incoming electrons is set to zero. Thus, the MTE calculated is purely

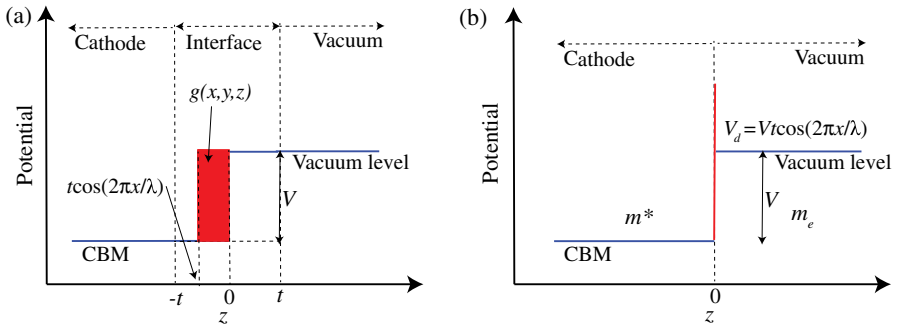

FIG. 5. (a) Potential to model the GaAs surface. The nonuniformities are modeled using a small sinusoidal roughness in the x direction. (b) The sinusoidal roughness is approximated using a δ function.

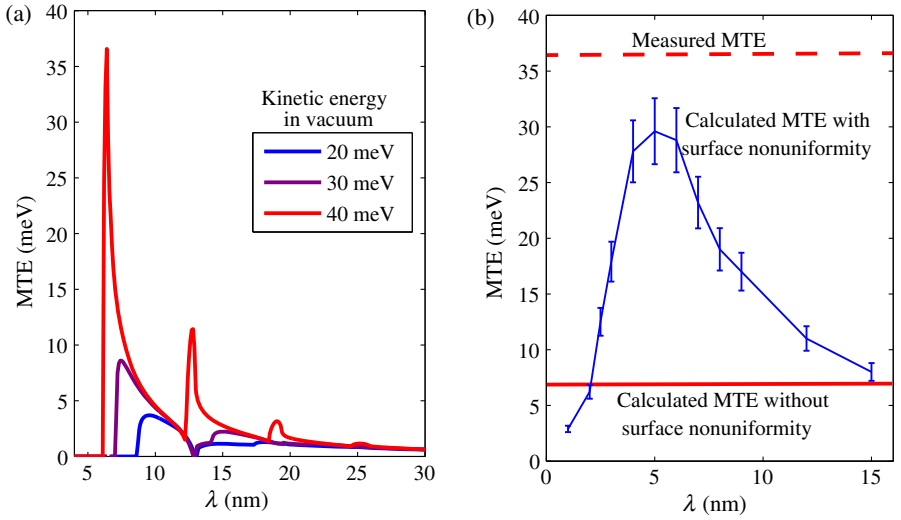

FIG. 6. (a) Calculated MTE as a function of the period (λ) of the surface nonuniformity for various electron energies. A spike in MTE occurs whenever the electron energy is sufficient to allow scattering into a higher-order transverse wave vector. (b) Calculated MTE as a function of the period (λ) for a realistic distribution of incoming wave vectors. The MTEs measured experimentally and calculated without the surface nonuniformity are also shown.

due to the effect of subnanometer-scale roughness. We can see that the MTE can increase with the increasing kinetic energy of the electrons.

A realistic distribution of the electron wave vectors emitted from the surface is calculated from the Monte Carlo–based electron transport simulation [18] for an incident photon energy of 1.6 eV. The MTE from such a distribution is calculated using Eq. (17) with $t = 1$ nm. Figure 6(b) shows this MTE for various values of λ. The MTE obtained experimentally and from the Monte Carlo simulation without assuming any surface scattering are also shown.

Scattering occurs only when the electron wavelength is comparable to the period of the surface nonuniformities. Hence, the MTE calculated using the quantum model for surface nonuniformities initially rises with increasing λ and then decreases. The MTE is comparable to the measured value if the period of nonuniformities is 4–6 nm. Thus, it is possible to explain the higher MTE measured from GaAs cathodes.

Although we discuss a specific case of GaAs cathodes, a similar argument can be made for any cathode material. Hence, to obtain very low MTE, it is necessary to make the surface devoid of subnanometer-scale roughness and essentially have an atomically perfect surface.

As the excess energy of the photons increases, electrons emitted have a higher kinetic energy and a smaller wavelength. For a kinetic energy equal to 0.2 eV, the de Broglie wavelength becomes lower than 3 nm, questioning the δ-function approximation. More general solutions to the scattering problem should be implemented to investigate this regime.

IV. CONCLUSION

We investigate the effect of surface nonuniformities on the MTE of photocathodes.

First, we develop a classical model to estimate the effect of the work-function variations on the MTE of emitted electrons. Using this model, we conclude that the surface work-function variations as low as 0.1–0.2 eV can at length scales of approximately 100 nm be sufficient to limit the MTE of emitted electrons to 20–30 meV (very close to the minimum measured value of 25 meV).

Second, we develop a quantum-mechanical model to study the effects of surface uniformities of a transverse spatial extent comparable to the wavelength of the emitted electrons. Using this model we show that subnanometer-scale surface roughness, atomic-scale surface defects, and surface reconstructions can affect the MTE significantly. Using NEA GaAs cathodes as an example, we show how such subnanometer-scale defects could limit the minimum measured MTE and account for various surface scattering effects.

Both of these effects have been ignored in photoemission models developed so far. The calculations presented here show that a detailed study of both these effects should be performed and included in photoemission models in order to explain photoemission accurately.

The detailed study of work-function variations on micron to nanometer scales, subnanometer-scale surface roughness, and surface structures is missing. These surface properties can change once the cathode samples are exposed to air. Hence, an *in situ* measurement of such surface characteristics of real photocathode surfaces is required to obtain accurate results. The calculations presented in this study show that the MTE from photocathodes may be limited by these effects, underscoring the importance of measuring these properties.

ACKNOWLEDGMENTS

The authors thank Laurent Boulet for his help with the classical part of the calculations and Dr. Dimitre Dimitrov for his helpful suggestions regarding the paper. This work is supported by the Department of Energy under Grant No. DE-SC0003965.

[1] I. V. Bazarov, B. M. Dunham, and C. K. Sinclair, Maximum Achievable Beam Brightness from Photoinjectors, Phys. Rev. Lett. **102**, 104801 (2009).

[2] P. Musumeci, J. T. Moody, C. M. Scoby, M. S. Gutierrez, H. A. Bender, and N. S. Wilcox, High quality single shot diffraction patterns using ultrashort megaelectron volt electron beams from a radio frequency photoinjector, Rev. Sci. Instrum. **81**, 013306 (2010).

[3] T. van Oudheusden, E. F. de Jong, S. B. van der Geer, W. P. E. M. Op t Root, O. J. Luiten, and B. J. Siwick, Electron source concept for single-shot sub-100 fs electron diffraction in the 100 kev range, J. Appl. Phys. **102**, 093501 (2007).

[4] J. M. Maxson, I. V. Bazarov, W. Wan, H. A. Padmore, and C. E. Coleman-Smith, Fundamental photoemission brightness limit from disorder induced heating, New J. Phys. **15**, 103024 (2013).

[5] I. V. Bazarov, B. M. Dunham, Y. Li, X. Liu, D. G. Ouzounov, C. K. Sinclair, F. Hannon, and T. Miyajima, Thermal emittance and response time measurements of negative electron affinity photocathodes, J. Appl. Phys. **103**, 054901 (2008).

[6] J. Feng, J. Nasiatka, W. Wan, T. Vecchione, and H. A. Padmore, A novel system for measurement of the transverse electron momentum distribution from photocathodes, Rev. Sci. Instrum. **86**, 015103 (2015).

[7] D. H. Dowell, I. Bazarov, B. Dunham, K. Harkay, C. Hernandez-Garcia, R. Legg, H. Padmore, T. Rao, J. Smedley, and W. Wan, Cathode R&D for future light sources, Nucl. Instrum. Methods Phys. Res., Sect. A **622**, 685 (2010).

[8] S. Karkare, L. Boulet, L. Cultrera, B. Dunham, X. Liu, W. Schaff, and I. Bazarov, Ultrabright and Ultrafast IIIV Semiconductor Photocathodes, Phys. Rev. Lett. **112**, 097601 (2014).

[9] T. C. Droubay, S. A. Chambers, A. G. Joly, W. P. Hess, K. Nemeth, K. C. Harkay, and L. Spentzouris, Metal-Insulator Photocathode Heterojunction for Directed Electron Emission, Phys. Rev. Lett. **112**, 067601 (2014).

[10] K. Nemeth, K. C. Harkay, M. van Veenendaal, L. Spentzouris, M. White, K. Attenkofer, and G. Srajer, High-Brightness Photocathodes through Ultrathin Surface Layers on Metals, Phys. Rev. Lett. **104**, 046801 (2010).

[11] D. H. Dowell and J. F. Schmerge, Quantum efficiency and thermal emittance of metal photocathodes, Phys. Rev. ST Accel. Beams **12**, 074201 (2009).

[12] T. Vecchione, D. Dowell, W. Wan, J. Feng, and H. A. Padmore, in *Proceedings of the 35th International Free Electron Laser Conference, New York, 2013* (Joint Accelerator Conferences Website, 2013), http://accelconf.web.cern.ch/AccelConf/fel2013/papers/tupso83.pdf.

[13] L. Cultrera, I. Bazarov, A. Bartnik, B. Dunham, S. Karkare, R. Merluzzi, and M. Nichols, Thermal emittance and response time of a cesium antimonide photocathode, Appl. Phys. Lett. **99**, 152110 (2011).

[14] I. Bazarov, L. Cultrera, A. Bartnik, B. Dunham, S. Karkare, Y. Li, X. Liu, J. Maxson, and W. Roussel, Thermal emittance measurements of a cesium potassium antimonide photocathode, Appl. Phys. Lett. **98**, 224101 (2011).

[15] L. Cultrera, S. Karkare, H. Lee, X. Liu, I. Bazarov, and B. Dunham, Cold electron beams from cryo-cooled, alkali antimonide photocathodes, arXiv:1504.05920.

[16] Tuo Li, Benjamin L. Rickman, and W. Andreas Schroeder, Emission properties of body-centered cubic elemental metal photocathodes, J. Appl. Phys. **117**, 134901 (2015).

[17] Tuo Li, Benjamin L. Rickman, and W. Andreas Schroeder, Density functional theory analysis of hexagonal close-packed elemental metal photocathodes, Phys. Rev. ST Accel. Beams **18**, 073401 (2015).

[18] S. Karkare, D. Dimitrov, W. Schaff, L. Cultrera, A. Bartnik, X. Liu, E. Sawyer, T. Esposito, and I. Bazarov, Monte Carlo charge transport and photoemission from negative electron affinity gaas photocathodes, J. Appl. Phys. **113**, 104904 (2013).

[19] R. L. Bell, *Negative Electron Affinity Devices* (Clarendon, Oxford, 1973).

[20] G. Vergara, A. Herrera-Gomez, and W. E. Spicer, Electron transverse energy distribution in GaAs negative electron affinity cathodes: Calculations compared to experiments, Surf. Sci. **436**, 83 (1999).

[21] S. Schubert, M. Ruiz-Oses, I. Ben-Zvi, T. Kamps, X. Liang, E. Muller, K. Muller, H. Padmore, T. Rao, X. Tong, T. Vecchione, and J. Smedley, Bi-alkali antimonide photocathodes for high brightness accelerators, APL Mater. **1**, 032119 (2013).

[22] H. J. Qian, C. Li, Y. C. Du, L. X. Yan, J. F. Hua, W. H. Huang, and C. X. Tang, Experimental investigation of thermal emittance components of copper photocathode, Phys. Rev. ST Accel. Beams **15**, 040102 (2012).

[23] S. Karkare and I. Bazarov, Effect of nanoscale surface roughness on transverse energy spread from gaas photocathodes, Appl. Phys. Lett. **98**, 094104 (2011).

[24] S. Karkare, L. Boulet, A. Singh, R. Hennig, and I. Bazarov, *Ab initio* studies of Cs on GaAs (100) and (110) surfaces, Phys. Rev. B **91**, 035408 (2015).

[25] S. Karkare, I. Bazarov, L. Cultrera, A. Iyer, X. Liu, and W. Schaff, in *Proceedings of the 24th Particle Accelerator Conference, PAC-2011, New York, 2011* (IEEE, New York, 2011).

[26] D. J. Bradley, M. B. Allenson, and B. R. Holeman, The transverse energy of electrons emitted from GaAs photocathodes, J. Phys. D **10**, 111 (1977).

[27] Th. Glatzel, S. Sadewasser, R. Shikler, Y. Rosenwaks, and M. Ch. Lux-Steiner (unpublished).

[28] W. Melitz, J. Shen, A. Kummel, and S. Lee, Kelvin probe force microscopy and its application, Surf. Sci. Rep. **66**, 1 (2011).

[29] C. Barth and C. R. Henry, Kelvin probe force microscopy on surfaces of UHV cleaved ionic crystals, Nanotechnology **17**, S155 (2006).

[30] Nicolas Gaillard, Denis Mariolle, Francois Bertin, Mickael Gros-Jean, and Ahmad Bsiesy, in *Symposium E Gate Stack Scaling Materials Selection, Role of Interfaces, and Reliability Implications*, MRS Proceedings Vol. 917 (Materials Research Society, Pittsburgh, 2006).

[31] H. Heil, Electron reflection coefficient at zero energy. II. Computer experiments on the reflection of slow electrons in the electrostatic field of surface patches, Phys. Rev. **164**, 887 (1967).

[32] E. A. Adler and R. T. Longo, Effect of nonuniform work function on space-charge-limited current, J. Appl. Phys. **59**, 1022 (1986).

[33] J. Robertson, Mechanisms of electron field emission from diamond, diamond-like carbon, and nanostructured carbon, J. Vac. Sci. Technol. B **17**, 659 (1999).

[34] Zhe Zhang and Chuanxiang Tang, Analytical study on emittance growth caused by roughness of a metallic photocathode, Phys. Rev. ST Accel. Beams **18**, 053401 (2015).

[35] E. Harier, C. Lubich, and G. Wanner, *Geometric Numerical Integration—Structure Preserving Algorithms for Ordinary Differential Equations*, Springer Series in Computational Mathematics (Springer, New York, 2006).

[36] W. E. Spicer, Negative affinity 35 photocathodes: Their physics and technology, Appl. Phys. A **12**, 115 (1977).

[37] Peter Johansson, Theory of interface-roughness scattering in resonant tunneling, Phys. Rev. B **48**, 8938 (1993).

[38] D. Z.-Y. Ting, E. T. Yu, and T. C. McGill, Multiband treatment of quantum transport in interband tunnel devices, Phys. Rev. B **45**, 3583 (1992).

[39] D. Z. Y. Ting, S. K. Kirby, and T. C. McGill, Interface roughness effects in resonant tunneling structures, Appl. Phys. Lett. **64**, 2004 (1994).

[40] D. Z. Y. Ting, S. K. Kirby, and T. C. McGill, Three dimensional simulations of quantum transport in semiconductor nanostructures, J. Vac. Sci. Technol. B **11**, 1738 (1993).

[41] W. T. Dietze and R. B. Darling, Coherent electron transport across semiconductor heterojunctions with rough interfaces, Phys. Rev. B **53**, 3925 (1996).

[42] H. C. Liu and D. D. Coon, Interface roughness and island effects on tunneling in quantum wells, J. Appl. Phys. **64**, 6785 (1988).

[43] Kai Sandfort, Ph.D. thesis, Karlsruher Institut für Technologie, 2010.

[44] S. Karkare, L. Cultrera, Y. Hwang, R. Merluzzi, and I. Bazarov, 2-d energy analyzer for low energy electrons, Rev. Sci. Instrum. **86**, 033301 (2015).